Space-Based Coherent Lidar for Wind Measurements with High-Percentage Tropospheric Coverage

Sammy Henderson and Don Jacob
Beyond Photonics, Boulder, CO, 80301, sammy@beyondphotonics.com

Abstract: We describe the potential for a 2-micron wavelength space-based coherent lidar system with power-aperture product and receiver efficiency sufficient to provide high percentage coverage tropospheric wind vector measurements along two continuous stripes in the atmosphere below the satellite track.

Keywords: Coherent Lidar, Wind Measurement

1. Introduction

Global measurements of altitude-resolved vector winds from an Earth-orbiting platform are of interest for both Earth science and weather forecasting applications. The potential for global wind measurements using lidar systems has been recognized for many years [1-3], and the technology has now advanced such that the first global wind measurement mission using direct detection Doppler lidar technology is scheduled to launch in late 2018 [4]. In recent years coherent lidar systems have primarily been considered for space-based wind measurements only in regions of the atmosphere where the aerosol backscatter is relatively high, e.g., the boundary layer and elevated aerosol layers higher in the troposphere. We describe the potential for a coherent detection wind lidar that has sufficient backscatter sensitivity to allow for high percentage coverage throughout the troposphere and lower stratosphere.

2. Coherently Detected Signal Photons and Diversity

As described in Frehlich's paper and elsewhere [2,5], the total number of backscattered photons that are detected by the coherent receiver over M_p pulses from a range gate of duration T_g is

$$\phi_T = \frac{\eta_{eo}\eta_a E T^2 \lambda \beta A_r M_p T_g}{2hR^2}. \quad (1)$$

In this equation, ϕ_T is the total number of coherently detected photons in the measurement, E is the pulse energy from the transmitter, T^2 is the two-way transmission to and from the target range, λ is the lidar wavelength, β is the aerosol backscatter coefficient at the lidar wavelength, A_r is the receiver aperture area, h is Planck's constant, R is the range to the center of the range gate, and $M_p = f_p T_m$ is the number of laser pulses used in the measurement, with f_p being the pulse repetition rate and T_m the total measurement time. The total efficiency of the coherent receiver is given by $\eta_{eo}\eta_a$, where η_{eo} is the electrooptic efficiency and η_a is the antenna efficiency. The electrooptic efficiency is $\eta_{eo} = \eta_{to}\eta_{ro}\eta_q\eta_{sn}$, and contains all the transmit and receive optical path losses other than the antenna efficiency loss, where the terms on the right-hand side of the equation are the efficiencies of the transmit and receive optics, detector quantum efficiency, and coherent detection shot noise efficiency respectively. The antenna efficiency contains losses due to transmit beam truncation, and mismatch between the wavefront of the received signal field and that of the local oscillator. Reduction of antenna efficiency occurs due to misalignments, wavefront aberrations in the lasers or optics, and atmospheric refractive turbulence.

Equation 1 can be inverted to solve for the backscatter coefficient. To determine the minimum detectable backscatter, we must determine the minimum number of coherently detected photons required to detect the signal in the presence of noise. Given that the effective noise of a coherent receiver is one coherently detected photon per diversity mode (aka, independent sample) [2], it is important to determine the total diversity in the measurement.

As the pulse travels through the atmosphere the coherent signal return exhibits well known temporal speckle fluctuations and the diversity, or number of statistically independent speckles, of the return in the range gate duration T_g is given by [6,7]

$$M_g = \left\{ \frac{\tau_{cg}}{T_\mathrm{g}} \mathrm{erf}\left(\sqrt{\pi} \frac{T_\mathrm{g}}{\tau_{cg}} \right) - \frac{1}{\pi} \left(\frac{\tau_{cg}}{T_\mathrm{g}} \right)^2 \left[1 - exp\left(-\pi \frac{T_\mathrm{g}^2}{\tau_{cg}^2} \right) \right] \right\}^{-1}, \quad (2)$$

where $\tau_{cg} = \int_{-\infty}^{\infty} |\mu_A(\tau)|^2 \, d\tau$, with τ_{cg} being the signal coherence time defined by Goodman [7] and $\mu_A(\tau)$ being the normalized signal autocorrelation function. For a Gaussian signal spectrum, which we assume for this analysis, the signal coherence time is given by $\tau_{cg} = 1/2\sqrt{\pi}\sigma_f$, where the total rms spectral width is $\sigma_f = \left(\sigma_{fT}^2 + \sigma_{fv}^2 \right)^{1/2}$, with $\sigma_{fT} = \sqrt{\ln 2}/(\sqrt{2}\,\pi\Delta T)$ being the rms spectral width of the assumed Gaussian temporal laser pulse with FWHM duration of ΔT, and σ_{fv} being the rms spectral width due to wind fluctuations (shear and turbulence) in the measurement volume.

In the limit that $T_\mathrm{g} \gg \tau_{cg}$ the range gate diversity becomes $M_g \approx T_\mathrm{g}/\tau_{cg}$, and if $T_\mathrm{g} \ll \tau_{cg}$ it becomes $M_g \approx 1$. In many measurement scenarios the approximation $M_g \approx T_\mathrm{g}/\tau_{cg}$ is sufficiently accurate and the total diversity of the measurement is $M_T = M_p M_g \approx f_p T_m T_g/\tau_{cg} = T_\mathrm{T}/\tau_{cg}$, where T_T is the total signal collection time for the measurement.

The detectability of the coherent lidar signal depends on the detectivity signal to noise ratio

$$SNR_d = \frac{\phi_T}{\sqrt{M_T}} = \sqrt{M_T} \cdot \frac{\phi_T}{M_T} = \sqrt{M_T} CNR_{MF} \, , \quad (3)$$

which is the mean height of the accumulated signal divided by the rms fluctuations of the accumulated noise floor. The matched filter carrier to noise ratio, CNR_{MF}, is the number of coherently detected photons per diversity mode. Using these relations, Equation 1 can be rewritten as

$$\beta = \frac{2hR^2 SNR_d}{\eta_{eo}\eta_a T^2 \lambda A_r \sqrt{T_m \cdot T_g \cdot \tau_{cg}} \cdot E \sqrt{f_p}} \, , \quad (4)$$

As will be shown below, the significance of SNR_d is that for moderate and high diversity levels the SNR_d required to detect the signal successfully is nearly constant.

3. Minimum Detectable Backscatter

The expression for backscatter illustrates that backscatter sensitivity is minimized by increasing the pulse energy, aperture area, signal coherence time, range gate time, and measurement time while decreasing the range. Higher pulse energy is more effective than higher pulse repetition rate. In order to determine the minimum detectable backscatter level that the lidar can sense, we must determine the minimum SNR_d at which the detection meets a given reliability, or probability of good estimates.

As described in the literature, detection of coherent lidar signals results in good detections at the actual signal location, and also detections that are randomly (uniformly) distributed across the search bandwidth (bad estimates) [5]. The minimum detectable backscatter depends on the fraction of uniformly spread bad estimates that is acceptable for the measurement. An integral equation providing an estimate of the fraction of bad estimates, P_b, is

$$P_b = \left(\frac{N_S}{N_S - 1} \right) (1 - P_{NA}) = \left(\frac{N_S}{N_S - 1} \right) \left\{ 1 - \int_{-\infty}^{\infty} pdf_{s+n}(y) \left[\int_{-\infty}^{y} pdf_n(x)\, dx \right]^{N_s - 1} dy \right\}. \quad (5)$$

We developed this and associated equations independently, but similar equations have been developed by others [8]. In this equation pdf_n and pdf_{s+n} are the probability density functions of the noise only and the signal plus noise respectively. At low to moderate total diversity the pdfs are both Gamma functions appropriate for accumulated coherently detected signals. At higher total diversity the signals are well approximated by Gaussian signals. The mean and variance of the noise only pdf is unity and $1/M_T$ rsspectively. and the mean and variance of the signal plus noise is $1 + CNR_{MF}$ and $(1 + CNR_{MF})^2/M_T$ respectively. When Gaussian pdfs are appropriate (i.e., at large total diversity) the integral equation is greatly simplified. Other terms in the integral equation are the number of search bins, N_S, which we define as the search bandwidth divided by the noise equivalent bandwidth of the signal, and P_{NA} which is the probability that the detection is in the signal bin, i.e., it is not an anomaly, which are any detections outside the signal bin. The $N_s/(N_s - 1)$ factor accounts for the fact that not all detections in the correct signal bin are actually good estimates.

An example of requirements that can be derived using Equation 5 are shown in Figures 1 and 2.

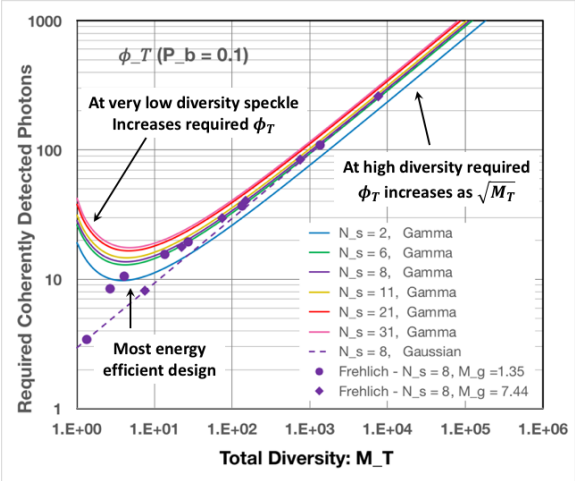

Figure 1. Coherently detected photons required to achieve 90% good estimates vs total diversity.

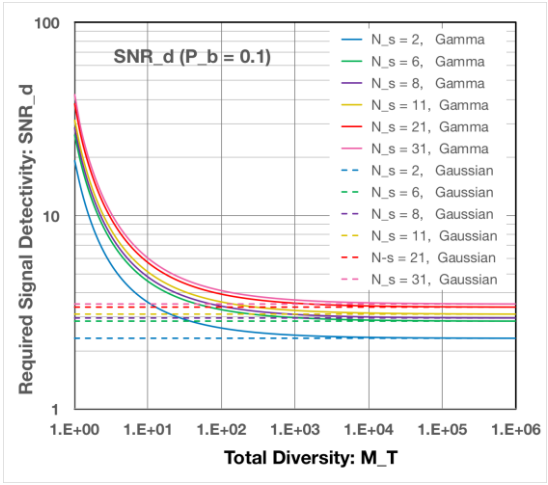

Figure 2. Signal detectivity required to achieve 90% good estimates vs. total diversity.

The lowest number of signal photons required to achieve $P_b = 0.1$ occurs for total diversity of 3-6, with the exact number depending on the number of search bins. Therefore, the total integrated transmitter energy required to make the measurement occurs at low diversity, with diversity sufficient to reduce speckle fades but not so high that more noise is introduced into the measurement. The $\sqrt{M_T}$ increase at higher diversity shown in the figure is a consequence of the effective coherent receiver noise of one detected photon per diversity mode. In general, coherent lidar systems are most energy efficient when a few coherently detected signal photons are detected from each signal coherence time, τ_{cg}, or diversity mode. But in many measurement scenarios this drives the required transmitter pulse energies to very high levels that are not easily obtained, so lower transmitter energy at higher pulse repetition rate is used with the penalty that the overall transmitted energy expended for the measurement increases.

Also shown in Figure 1 are the number of coherently detected photons required as calculated using the complicated analytic fit equations that Frehlich developed [5]. At higher total diversity (> 10) these calculated points using the Frehlich equations match very well the values calculated from the simpler Equation 5. At lower total diversity there is significant disagreement which indicates that the Frehlich analytic fit equation are not valid at very low diversity, which is reasonable as he indicates in the paper that simulations with 10 pulse averaging were the lowest considered in his analysis.

The SNR_d required to achieve $P_b = 0.1$ parametric in the number of search bins is shown in Figure 2, using both the exact Gamma statistics and the Gaussian approximation. This again illustrates that the Gaussian approximation is accurate for high diversity but cannot be used at lower diversity. When the total diversity is above about 500 the required SNR_d flattens to the fixed values predicted by the Gaussian pdfs. The invariance of the required SNR_d level at higher diversities illustrates that it is a valuable fundamental parameter for determining the performance of coherent lidar systems.

Similar requirements like those shown in Figures 1 and 2 and others can be generated at any bad estimate probability value using Equation 5. Once the required SNR_d to achieve a given probability of bad estimates is determined, and the other lidar parameters are defined, Equation 4 can be used to determine the minimum backscatter level consistent with this level of bad estimates.

4. Velocity Precision

A lower bound of velocity measurement error for the good estimates (not including the uniformly distributed bad estimates) is given by the Cramer Rao Lower Bound (CRLB) [2]. Written in terms of the total number of coherently detected photons and total diversity the CRLB is given by

$$var[V_r] \geq \left(\frac{\lambda}{2}\right)^2 \sigma_f^2 \left[\frac{2}{\phi_T} + \frac{2M_T}{\phi_T^2} + \frac{1}{2M_T}\right] . \quad (6)$$

When the coherently detected photons per diversity mode is small (i.e., $\phi_T \ll M_T$), then the middle term dominates, and the CRLB is well approximated by $var[V_r] \geq \left(\frac{\lambda}{2}\right)^2 \sigma_f^2 \frac{2M_T}{\phi_T^2} = \frac{\lambda^2 \sigma_f^2}{2SNR_d^2}$.

With well-designed frequency (velocity) estimation algorithms optimized for low signal levels achieving performance close to that predicted by Equation 6 at low signal levels has been demonstrated. For typical coherent lidar designs considered for space-based wind measurement applications, as long as the backscatter is sufficient for measurements to be made with acceptable probability of bad estimates, the velocity precision will be 1-2 m/s. Of course, even higher precision is possible if the backscatter is well above the minimum detectable levels.

5. High-Sensitivity Space-Based Coherent Lidar

Our objective in this investigation was to conceptually design a coherent lidar that could measure winds from a space-based platform at very low backscatter levels. Past aerosol backscatter measurements imply that a 2 μm wavelength coherent lidar with backscatter sensitivity of $\sim 10^{-10}(m \cdot sr)^{-1}$ would be able to make useful measurements in the upper troposphere and lower stratosphere a large fraction of the time (possibly as high as 80-90% of the time).

In order to measure horizontal wind vectors multiple look directions are required. For space-based wind measurements, overlaid fore and aft tracks produce robust radial wind measurements along each line of sight (LOS) direction and therefore can be combined to reliably produce horizontal vector measurements along one track in the atmosphere. To allow for measurements along two tracks below the flight path, four look directions are required. Many system concepts assume multiple telescopes looking in each LOS direction, which is reasonable for small optics size but is not desirable for meter class telescopes. A feasible strawman design for a system that can achieve high backscatter sensitivity over four look directions is summarized below and will be described in more detail in the presentation.

The transmitter is an in-band-pumped Ho:LuLF laser operating at a high atmospheric transmission wavelength near 2 μm. The laser front end produces 80 mJ, 180 ns FWHM pulses at 100 Hz PRF (similar laser is currently under development under NASA's Wind-SP program). Alternate pulses from the front-end laser are optically switched into two paths with each path having a high-efficiency in-band-pumped amplifier operating at 50 Hz PRF. The high energy amplifiers require development to optimize efficiency and beam quality but similar performance has previously been demonstrated in Ho:YLF [9]. Following alternate pulse recombination, the final transmitter output is 240 mJ at 100 Hz. With optimization, the overall high-power transmitter wall plug efficiency is expected to be ~3%, so the overall spacecraft prime power required by the transmitter is <1 kW.

Lidar sensitivity is significantly enhanced by using a 1.5 m aperture diameter and 320 km orbit altitude (*same as ESA Aeolus*). An EO-tunable aperture at the telescope output based on pulse-to-pulse polarization control and liquid crystal polarization gratings, toggles the lidar line of sight at the laser PRF sequentially across four lines of sight (fore and aft views for each of the two stripes) with each line of sight operating at 25 Hz PRF. In this concept the polarization gratings are in large beam at the output of the telescope. The polarization gratings are very efficient and have been demonstrated in coherent lidar systems [10], but development is required to scale the technology to large apertures.

To predict the minimum backscatter sensitivity, we also assume a high-efficiency lidar design with $\eta_{eo}\eta_a = 16\%$, rms wind turbulence and shear in the measurement volume of 2 m/s, LOS angles that are ~ 28.4° from nadir (results in 60° elevation wrt to Earth surface), and a LOS velocity search space of ~ 60 m/s ($N_s = 11$). Achieving 16% total lidar efficiency requires that optical transmission and detector quantum efficiency be maximized, wavefront aberrations be minimized, and lag angle due to platform rotations be removed or greatly minimized. The approach planned to maximize the lidar efficiency is described in a separate paper [11]. The lidar model we use is very detailed, including the atmospheric attenuation, refractive turbulence, and antenna efficiency variation with range.

Example model results are shown in Figures 3. The minimum detectable backscatter is shown for probability of bad estimates of 0.5, 0.1, and 0.02 and for both high and low measurement resolutions. For the high-resolution measurement (red solid squares under lines) the height resolution is 250 m and

the horizontal resolution is 11 km (1.5 s accumulation). For the low-resolution measurement (black squares under lines) the height resolution is 2 km and the horizontal resolution is 88 km (12 s accumulation). Also shown for comparison are various measurement-based backscatter coefficient models we use in our lidar modeling. The clean air model, solid blue line with open blue circles, represents very clean air with past measurements indicating that aerosol backscatter will be above this level 80-90% of the time. The lidar described above allows for accurate wind measurements to minimum backscatter coefficient of ~ 10^{-10}/m/sr for 1 km vertical x 88 km horizontal resolution, providing high-percentage coverage at acceptable resolution for the mid- and upper-troposphere; and to minimum of ~10^{-9}/m/sr for 250 m vertical x 11 km horizontal resolution, allowing for high resolution measurements in the boundary layer and in enhanced aerosol layers in mid- and upper-troposphere. Of course, at high backscatter levels, even higher resolution measurements are possible with the coherent lidar. For example, with only 3 shot averaging, measurements can be made to 50 m vertical x 0.88 km horizontal resolution as long as the aerosol backscatter is above ~10^{-8}/m/sr. So very high-resolution boundary layer wind measurements are possible even under very clear air conditions. The lidar architecture and additional modeling will be described in more detail in the presentation.

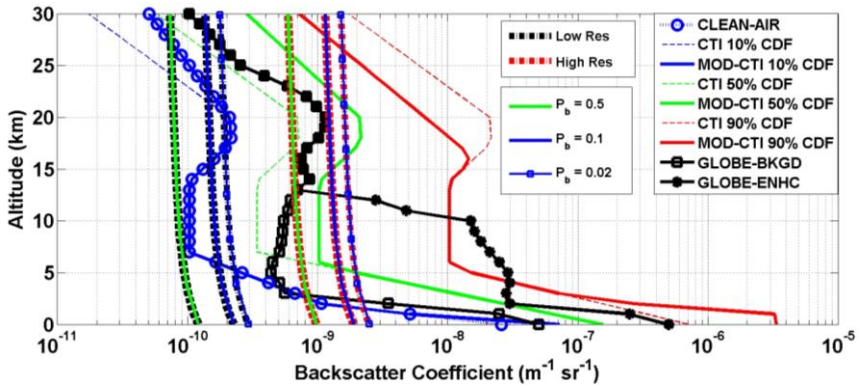

Figure 3. Predicted minimum detectable backscatter levels and measurement-based model backscatter profiles.

Figure 4. Nonmechanical beam scanning concept.

6. Acknowledgments

Michael Kavaya provide the predictions from the Frehlich paper that were included in Figure 1.

7. References

[1] R.M. Huffaker, et.al., "Feasibility studies for a global wind measuring satellite system (Windsat): Analysis of simulated performance," Appl. Opt., 23, 2523-2536, 1984

[2] S.W. Henderson, et.al, "Wind Lidar" in *Laser Remote Sensing*, T. Fujii and T. Fukuchi, Eds., CRC Taylor and Francis, 469-722 (2005)

[3] W. E. Baker, eta.al., "Lidar-Measured Wind Profiles: The Missing Link in the Global Observing System," Bulletin of the American Meteorological Society, Vol 95, No 4, (2014)

[4] A.M Dabas, et,al., "ESA wind lidar mission Aeolus", 19th Coherent Laser Radar Conference, paper Mo2, Okinawa, Japan (2018)

[5] R. Frehlich, "Velocity Error for Coherent Doppler Lidar with Pulse Accumulation," Journal American Meteorological Society, Vol 21, 905-920, (2004)

[6] D. Jacob and P. Gatt, "Defining CNR, Diversity, Window Efficiency, and Resolution of Coherent Lidar for Optimizing System Performance", in proceedings of 16th Coherent Laser Radar Conference

[7] Goodman, J.W., Statistical Optics: An Introduction, New York: Wiley, 1984.

[8] Shapiro, J.W. et.al., "Performance analysis of peak-detecting laser radars," SPIE Vol. 663, pp 38-56, (1986)

[9] H.J Strauss, et.al., "330 mJ single-frequency Ho:YLF slab amplifier," Opt. Lett., Vol 38, 1022 (2013)

[10] S. Serati, et.al., "Large-aperture, wide-angle nonmechanical beam steering using polarization gratings", *Opt. Eng*. 56(3), 031211 (Oct 27, 2016). Also see paper We7 in this conference.

[11] S.W. Henderson, "Antenna Efficiency Optimization in Coherent Lidar Systems" 19th Coherent Laser Radar Conference, paper Tu2, Okinawa, Japan (2018)